Phase Mismatch–Free Nonlinear Propagation in Optical Zero-Index Materials

Haim Suchowski,[1]* Kevin O'Brien,[1]* Zi Jing Wong,[1]* Alessandro Salandrino,[1] Xiaobo Yin,[1,2] Xiang Zhang[1,2]†

Phase matching is a critical requirement for coherent nonlinear optical processes such as frequency conversion and parametric amplification. Phase mismatch prevents microscopic nonlinear sources from combining constructively, resulting in destructive interference and thus very low efficiency. We report the experimental demonstration of phase mismatch–free nonlinear generation in a zero-index optical metamaterial. In contrast to phase mismatch compensation techniques required in conventional nonlinear media, the zero index eliminates the need for phase matching, allowing efficient nonlinear generation in both forward and backward directions. We demonstrate phase mismatch–free nonlinear generation using intrapulse four-wave mixing, where we observed a forward-to-backward nonlinear emission ratio close to unity. The removal of phase matching in nonlinear optical metamaterials may lead to applications such as multidirectional frequency conversion and entangled photon generation.

Nonlinear optics, the study of phenomena occurring when optical properties of a material are modified by the presence of light, plays a critical role in frequency conversion, nonlinear spectroscopy, and the generation of new light sources (*1*, *2*). A major problem in nonlinear optics is the inherent phase mismatch between the interacting waves propagating inside the nonlinear materials. This effect originates from material dispersion and causes a lack of optical momentum conservation between the photons involved in the nonlinear process. The phase mismatch prevents the constructive addition of the nonlinear fields, resulting in destructive interference and poor generation efficiency. To increase the amounts of nonlinear light, a compensation technique must be used. The most widely used methods (Fig. 1A) include birefringent phase matching, angle phase matching, and quasi–phase matching (*3*–*6*). Implementing each technique poses a number of challenges. The birefringent phase-matching technique uses the polarization-dependent indices to match the phase velocities of the interacting waves, but it is limited to birefringent materials (*1*, *2*). Angle phase matching uses geometrical alignments of the interacting waves to compensate the phases, but the noncollinear optical arrangement limits the interaction length (*1*, *2*). Quasi–phase matching cancels out the inherent phase mismatch using artificial momentum introduced by periodic and/or aperiodic poling of nonlinear crystals, which is restricted to certain nonlinear crystals and provides a limited range of mismatch that can be compensated. Moreover, all compensating schemes work only in a specific direction: either in the forward direction (*3*–*6*) or the backward direction (*7*, *8*), but not both. This restriction arises because the phase-matching process represents a balance between the momenta of the photons involved in the nonlinear interaction—a balance that is disturbed when the momentum of one photon changes sign because of a direction change.

We show that the requirement for phase matching can be eliminated using a metamaterial with a zero refractive index. In a zero-index material (*9*–*11*), the photons carry zero momentum and satisfy momentum conservation for any combination of photon directions, thereby allowing the nonlinearly generated waves to coherently build up in both forward and backward directions. We demonstrate the nonlinear dynamics through four-wave mixing (FWM) in a metamaterial with zero refractive index. Equal amounts of nonlinearly generated waves are observed in

[1]NSF Nanoscale Science and Engineering Center, University of California, Berkeley, CA 94720, USA. [2]Materials Sciences Division, Lawrence Berkeley National Laboratory, Berkeley, CA 94720, USA.

*These authors contributed equally to this work.
†Corresponding author. E-mail: xiang@berkeley.edu

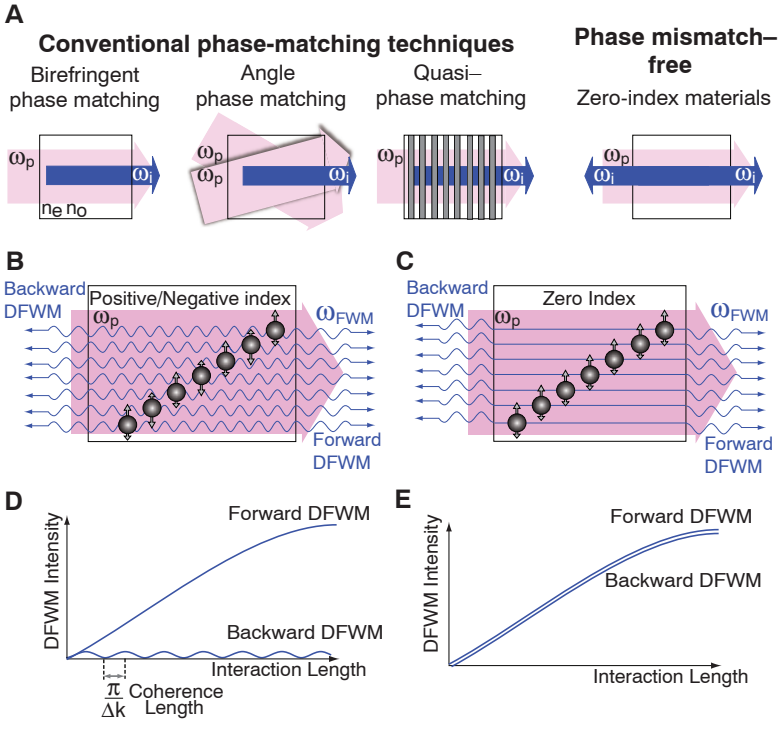

Fig. 1. The role of phase mismatch. Avoiding phase mismatch is critical for obtaining efficient nonlinear conversion. (**A**) The most widely used methods for phase matching—birefringence phase matching, angle phase matching, and quasi–phase matching—allow compensation either in the forward or backward directions, but not both. (**B** to **E**) In contrast, a zero-index metamaterial creates a phase mismatch–free environment for nonlinear propagation, eliminating the requirement for phase matching. In the microscopic picture of nonlinear generation, each source coherently emits equally in both directions, acquiring a phase that is proportional to the refractive index [(B) and (C)] as it propagates. All of these sources add up coherently to generate the net nonlinear emission. In a zero-index medium (C), the radiations from all nonlinear sources acquire no phase as they propagate, guaranteeing a constructive interference and an increase of the signal in both directions with propagation length (E). In contrast, in a finite-index medium (B), the emission acquires phase as it propagates, leading to destructive interference when the process is not phase-matched. For example, in a degenerate four-wave mixing (FWM) process in which $\omega_{signal} \approx \omega_{pump} \approx \omega_{idler}$, the sources destructively interfere in the backward direction (D), resulting in weaker backward emission.

both forward and backward propagation directions, matching well with the predictions from nonlinear scattering theory (*12*). In contrast, the forward and backward FWM generations are drastically different for metamaterials with a positive or a negative index, as expected from phase-matching considerations.

Metamaterials allow us to tailor the linear electromagnetic response and introduce new regimes of interaction between radiation and matter (*13*–*17*). The nonlinear properties of negative-index metamaterials have been explored both theoretically (*18*–*21*) and experimentally (*22*–*26*). The rich nonlinear dynamical behavior in metamaterials promises the realization of novel effects such as backward mirrorless parametric amplification (*18*, *19*), novel quantum switches (*20*), and cavity-free microscopic optical parametric oscillators (*21*).

To illustrate the phase mismatch–free nonlinear wave interactions in a zero-index material, we consider a degenerate FWM process in which the pump, signal, and idler photons have approximately the same wavelength ($\omega_{signal} \approx \omega_{pump} \approx \omega_{idler}$). In this process, the phase (momentum) mismatch in the forward and backward propagation directions can be expressed as $\Delta k_{\pm} = |2k_{pump} - k_{signal} \mp k_{idler}|$, where the plus and minus subscripts represent the forward and backward directions, respectively. In a conventional degenerate FWM system, when one of the propagation directions, say the forward direction, is perfectly phase-matched (i.e., $\Delta k_{+} \to 0$), the phase is then poorly matched in the backward propagation direction where $\Delta k_{-} \approx 2|k_{idler}|$. For a metamaterial with a zero refractive index at the idler frequency, however, the phase mismatch in both the forward and backward directions is zero. This important distinction between forward and backward nonlinear propagation allows us to explore nonlinear generation for negative-, positive-, and zero-index regimes. We expect that in the case of negative or positive index, because $\Delta k_{+} \to 0$ while $\Delta k_{-} \neq 0$, the generated forward light is accumulated in phase while the generated backward light is not, thus causing the degenerated FWM intensity to grow monotonically for the forward direction and to oscillate for the backward direction (Fig. 1, B and D). In contrast, in the zero-index regime, $\Delta k_{+} \to 0$ and also $\Delta k_{-} \to 0$, making both the generated forward light and backward light accumulate in phase, having the same yield in the forward and backward directions (Fig. 1, C and E). This is in stark contrast to nonlinear generation in negative-index materials, where the phase mismatch parameter has a finite value (*18*–*21*). A phase mismatch–free zero-index material allows the nonlinear process to be efficient regardless of directionality, and the need to carefully balance between the momenta of the waves involved in the nonlinear interaction is eliminated. In our experimental realization, the pump pulse has a positive Poynting vector in the material, so the direction of energy flux is the same as in free space. In contrast, the nonlinear emission has an energy flux in both directions, with the relative amounts influenced by the phase matching. The refractive index controls the direction of the phase velocity and canonical momentum relative to the direction of the energy flux (*13*, *27*), which influences the direction of energy propagation through the phase matching. In a zero-index medium, as seen, the energy flux in both directions is equal. Relative to the poorly phase-matched case, more energy will be extracted from the pump in a zero-index material.

Figure 2A shows the experimental apparatus for single-shot FWM, which allows intrapulse wave mixing between the different spectral components of ultrashort pump laser pulses (*28*). Before impinging on the samples, the transform-limited pump pulse is amplitude-shaped to remove the long-wavelength tail in the spectral domain. The generated intrapulse FWM is measured in both forward and backward directions within this filtered spectral regime. This method eliminates the need to overlap two laser pulse temporally and spatially, and maximizes the nonlinear yield (see fig. S3). An example measurement spectrum (Fig. 2B) shows both the generated FWM signal and the pump with their relative strengths. Note that the pump is far from depleted by the nonlinear process, as evident from the much weaker FWM signal than that of the pump. Operating in the weak-field regime (the generated intensity of the idler is on the order of 10^{-5} of the pump intensity) allows us to analyze the experimental observations with a perturbative approach. We verify the nonlinear origin of the emission by measuring the cubic scaling with pump power and quadratic spectral phase dependence (see supplementary materials).

We have chosen the fishnet metamaterial structure (*9*), a stack of metal-dielectric multilayers with perforated holes (Fig. 2). Fishnet metamaterials are widely used negative-index materials at optical frequencies because of their low loss, well-understood linear properties, and robust fabricability. Our fishnet metamaterial consists of 20 alternating 30-nm gold and 50-nm magnesium fluoride layers on a 50-nm-thick silicon nitride membrane. The magnetic moments (created by the antiparallel currents in neighboring conductive layers) and the electric responses of the perforated metallic thin films provide a positive, zero, or negative refractive index regime, depending on the wavelength. We measured the transmission and refractive index by spectrally and spatially resolved interferometry (*29*), which measures simultaneously the phase for an ultra-broadband optical range to an accuracy of greater than $\lambda/300$ (fig. S1). The zero crossing of the index is approximately 1325 to 1340 nm for the sample with period of 750 nm

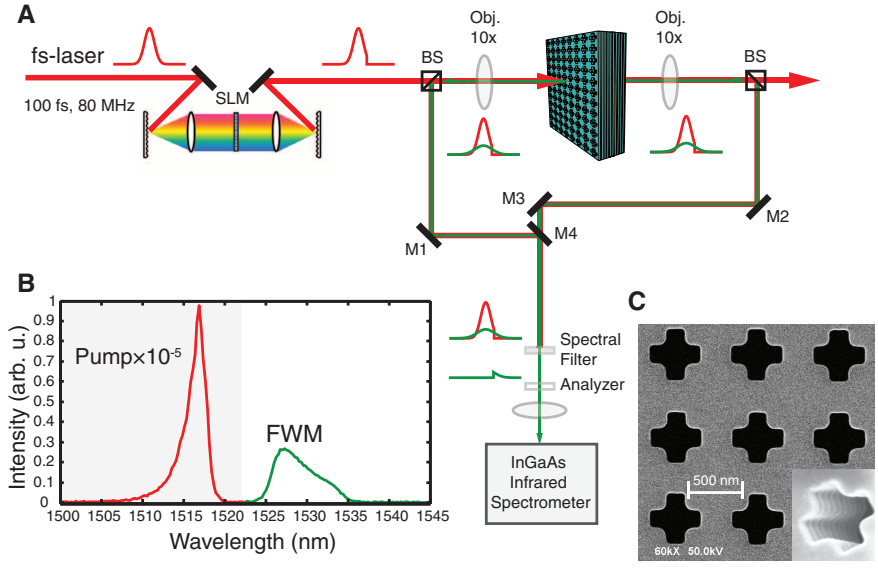

Fig. 2. Experimental apparatus for nonlinear measurements. (**A**) A transform-limited 100-fs laser pulse centered at 1315 nm or 1510 nm is amplitude-shaped through a spatial light modulator (SLM) to remove the long-wavelength tail of the pulse (red). The pulse is passed through a fishnet metamaterial, which generates a FWM nonlinear signal (green) in the backward and forward directions because of a third-order nonlinearity. The FWM signals are measured in an infrared spectrometer after filtering the pump pulse. The forward emission is measured without the flip mirror (M4). An analyzer is used before the spectrometer to control the detected polarization; a half-wave plate (not shown) controls the pump polarization. (**B**) An example measurement of the emission spectrum, showing both the generated FWM signal (green) and the filtered pump (red). The pump is undepleted by the nonlinear process, as evident by the much weaker FWM signal than that of the pump (the magnitude of the FWM is ~10^{-5} times the pump intensity), justifying the use of the perturbative approach in our analysis. (**C**) Scanning electron micrograph of the cross-fishnet structures. Inset shows an angled view. See supplementary materials for details of the single-shot FWM method.

and cross lateral holes of dimensions 475 nm × 175 nm (Fig. 2C). Using the measured refractive index values of the fishnet structures, the phase mismatch values can be calculated as a function of wavelength for forward and backward propagation (Fig. 3A). The forward phase mismatch is $\Delta k_+ \rightarrow 0$ for all wavelengths, whereas Δk_- has different values across the zero-index wavelength. However, in the wavelength regime of zero refractive index (~1330 nm), both the forward and backward directions are phase mismatch–free.

The intrapulse FWM signal in the zero-index regime (where the refractive index changes its sign) is shown for both the forward and the backward directions (Fig. 3B). The observed nonlinear yield is about the same in both directions. In contrast, in the negative-index regime, the intensities of the degenerate FWM signals in the opposite propagation directions are distinctly different (Fig. 3C). Because of the low transmission at 1530 nm, a different fishnet metamaterial with 800-nm period and perforated hole size of 560 nm by 250 nm was used. The zero crossing of the refractive index is at ~1460 nm and the refractive index is –0.5 at 1530 nm (fig. S1). The relative strength of the forward and backward FWM waves correlates with the predicted phase-matching difference for zero and negative indices, as illustrated in Fig. 1. In particular, at the zero refractive index, the observation of a forward/backward FWM ratio of unity indicates phase mismatch–free nonlinear interaction for both directions. Low transmission loss is critical for observing the effects of phase matching. High losses can also strongly affect the ratio of the forward and backward nonlinear emission for positive-, negative-, and zero-index regimes. Loss decreases the overall nonlinear emission and, because of the shorter propagation length of backward emission, increases the backward emission relative to the forward. The fabricated fishnet has a relatively low loss in the zero-index regime, allowing us to observe the effects of phase matching rather than absorption.

The phase mismatch–free nonlinear generation can be further demonstrated by measuring the nonlinear emission as a function of the polarization angle of the pump for the forward and backward FWM, shown in the insets of Fig. 3, B and C, for the zero-index and negative-index materials, respectively. The relative strength between the forward and backward nonlinear waves in the zero-index region is again about the same for all polar angles, whereas in the negative-index regime, the forward nonlinear waves remain stronger than the backward for all polarizations. The polarization-dependent FWM (with a horizontally polarized analyzer) matches well the analytical curve of $\cos^6 \theta$, a characteristic response of a third-order nonlinearity intensity signal. This angular dependence is particularly important, as it means that the nonlinearity originates from the light that is coupled into the metamaterial (see supplementary materials).

A numerical simulation of the dynamics as a function of thickness around the zero index predicts a ratio of unity for forward/backward nonlinear emission (fig. S2A), whereas in the negative-index regime, the forward generated nonlinear signal has a much higher yield than that of the backward signal (fig. S2B) for a thick fishnet of 20 layers. In contrast, for thin fishnets (fewer than five layers), the forward/backward ratio is unity regardless of the index of refraction, indicating that phase matching is not important in these structures (*23*–*26*). The nonlinear simulation is performed with nonlinear scattering theory (*12*), which calculates the nonlinear properties using the linear results from a full wave simulation of the metamaterial, taking into account the fabricated structure geometry and material losses. To further confirm that phase plays a dominant role in the dynamics with respect to loss or surface effects, we artificially removed the phase mismatch in the nonlinear simulation while keeping loss, thus forcing all waves to add up constructively. We found that the behavior in the zero-index region is unchanged, indicating that phase matching plays little role. In contrast, in the negative-index region, the forward and backward emissions became nearly equal, indicating that phase matching is critical in this region. Note that perfect phase matching using a zero refractive index is different from quasi–phase matching (*4*, *22*), in which the effective momentum supplied by a periodic structuring is used to compensate for a phase mismatch. In these experiments, the subwavelength spacing of the layers (80 nm) does not provide sufficient effective momentum to phase-match the backward nonlinear generation (see fig. S7).

The concept of phase mismatch–free nonlinear interaction in zero-index materials provides a new degree of freedom in controlling the nonlinear dynamics in a metamaterial and can be further explored in other nonlinear processes such as coherent Raman spectroscopy for remote sensing applications or spontaneous parametric down-conversions for entangled photon generation. The design of multivalued or broadband zero-index materials opens the opportunity to achieve phase mismatch–free dynamics for simultaneous nonlinear processes.

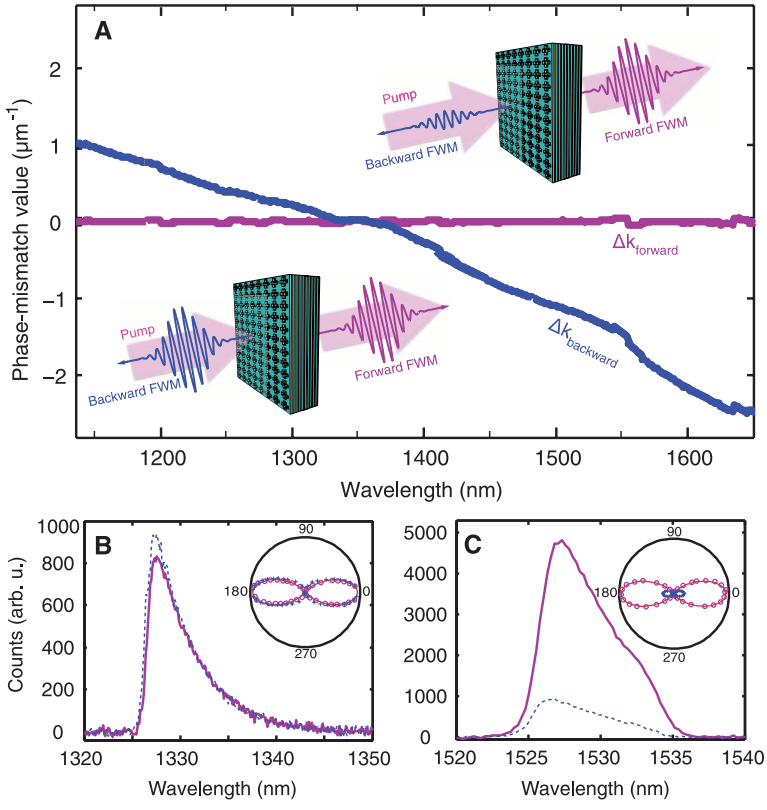

Fig. 3. Four-wave mixing in metamaterials with and without phase mismatch. (**A**) Phase mismatch of forward (purple) and backward (blue) FWM as a function of wavelength, based on experimentally measured refractive indices. The forward phase mismatch is near zero ($\Delta k_+ \rightarrow 0$) for all wavelengths; the backward has a large phase mismatch ($\Delta k_- \neq 0$) except when the index is near zero. (**B**) The measured FWM process in the zero-index regime has almost the same yield in both directions, illustrating the phase mismatch–free properties of zero-index materials. (**C**) In contrast, the forward-propagating FWM (solid purple) is much stronger than the backward (dashed blue) in the negative-index regime as a result of the phase mismatch. Insets in (B) and (C) show the dependence of the nonlinear emission (with a horizontally polarized analyzer) on pump polarization, which has the characteristic $\cos^6 \theta$ curve of $\chi^{(3)}$ dynamics. The nonlinear emission scales with the cube of the pump power and shows a spectral phase dependence demonstrating the nonlinear origin (fig. S6).

References and Notes

1. Y. R. Shen, *The Principles of Nonlinear Optics* (Wiley-Interscience, New York, 1984).
2. R. Boyd, *Nonlinear Optics* (Academic Press, New York, ed. 3, 2008).
3. J. A. Armstrong, N. Bloembergen, J. Ducuing, P. S. Pershan, *Phys. Rev.* **127**, 1918–1939 (1962).
4. D. S. Hum, M. M. Fejer, *C. R. Phys.* **8**, 180–198 (2007).
5. A. Arie, N. Voloch, *Laser Photonic Rev.* **4**, 355–373 (2010).
6. A. Rose, D. R. Smith, *Opt. Mater. Express* **1**, 1232–1243 (2011).
7. X. Gu, R. Y. Korotkov, Y. J. Ding, J. U. Kang, J. B. Khurgin, *J. Opt. Soc. Am. B* **15**, 1561–1566 (1998).
8. C. Canalias, V. Pasiskevicius, *Nat. Photonics* **1**, 459–462 (2007).
9. J. Valentine *et al.*, *Nature* **455**, 376–379 (2008).
10. C. Argyropoulos, P. Y. Chen, G. D'Aguanno, N. Engheta, A. Alù, *Phys. Rev. B* **85**, 045129 (2012).
11. E. J. R. Vesseur, T. Coenen, H. Caglayan, N. Engheta, A. Polman, *Phys. Rev. Lett.* **110**, 013902 (2013).
12. S. Roke, M. Bonn, A. V. Petukhov, *Phys. Rev. B* **70**, 115106 (2004).
13. V. G. Veselago, *Sov. Phys. Solid State* **8**, 2854–2856 (1967).
14. J. B. Pendry, *Phys. Rev. Lett.* **85**, 3966–3969 (2000).
15. R. A. Shelby, D. R. Smith, S. Schultz, *Science* **292**, 77–79 (2001).
16. V. M. Shalaev, *Nat. Photonics* **1**, 41–48 (2007).
17. N. Fang, H. Lee, C. Sun, X. Zhang, *Science* **308**, 534–537 (2005).
18. A. K. Popov, V. M. Shalaev, *Appl. Phys. B* **84**, 131–137 (2006).
19. A. K. Popov, V. M. Shalaev, *Opt. Lett.* **31**, 2169–2171 (2006).
20. A. K. Popov, S. A. Myslivets, V. M. Shalaev, *Opt. Lett.* **34**, 1165–1167 (2009).
21. M. Scalora *et al.*, *Opt. Express* **14**, 4746–4756 (2006).
22. A. Rose, D. Huang, D. R. Smith, *Phys. Rev. Lett.* **107**, 063902 (2011).
23. S. Tang *et al.*, *Opt. Express* **19**, 18283–18293 (2011).
24. K. M. Dani *et al.*, *Nano Lett.* **9**, 3565–3569 (2009).
25. A. Minovich *et al.*, *Appl. Phys. Lett.* **100**, 121113 (2012).
26. J. Reinhold *et al.*, *Phys. Rev. B* **86**, 115401 (2012).
27. S. M. Barnett, *Phys. Rev. Lett.* **104**, 070401 (2010).
28. N. Dudovich, D. Oron, Y. Silberberg, *Nature* **418**, 512–514 (2002).
29. K. O'Brien *et al.*, *Opt. Lett.* **37**, 4089–4091 (2012).

Acknowledgments: Supported by the U.S. Department of Energy, Office of Basic Energy Sciences, under contract no. DE-AC02-05CH11231 through the Materials Sciences Division of Lawrence Berkeley National Laboratory. H.S. and Z.J.W. acknowledge partial support by the Fulbright Foundation. We thank the Molecular Foundry, Lawrence Berkeley National Laboratory, for technical support in nanofabrication.

Supplementary Materials

www.sciencemag.org/content/342/6163/1223/suppl/DC1
Materials and Methods
Figs. S1 to S8
References (*30*–*33*)

6 August 2013; accepted 21 October 2013
10.1126/science.1244303

Interfollicular Epidermal Stem Cells Self-Renew via Autocrine Wnt Signaling

Xinhong Lim,[1]* Si Hui Tan,[2] Winston Lian Chye Koh,[3] Rosanna Man Wah Chau,[3] Kelley S. Yan,[4] Calvin J. Kuo,[4] Renée van Amerongen,[1]† Allon Moshe Klein,[5]‡ Roel Nusse[1]‡

The skin is a classical example of a tissue maintained by stem cells. However, the identity of the stem cells that maintain the interfollicular epidermis and the source of the signals that control their activity remain unclear. Using mouse lineage tracing and quantitative clonal analyses, we showed that the Wnt target gene *Axin2* marks interfollicular epidermal stem cells. These *Axin2*-expressing cells constitute the majority of the basal epidermal layer, compete neutrally, and require Wnt/β-catenin signaling to proliferate. The same cells contribute robustly to wound healing, with no requirement for a quiescent stem cell subpopulation. By means of double-labeling RNA in situ hybridization in mice, we showed that the *Axin2*-expressing cells themselves produce Wnt signals as well as long-range secreted Wnt inhibitors, suggesting an autocrine mechanism of stem cell self-renewal.

Stem cells residing in the adult interfollicular epidermis (IFE) regenerate the skin, but the nature of these cells and the molecular signals that regulate them remain incompletely understood. Because of their well-established importance in stem cell maintenance and hair growth, Wnts are candidate self-renewal factors for IFE stem cells. However, Wnt/β-catenin signaling is generally thought to control IFE differentiation rather than self-renewal (*1*, *2*). Reinforcing this view, interfollicular epidermal stem cells (IFESCs) have recently been suggested to originate from more primitive Wnt-independent ($Lgr6^+$) stem cells residing in the hair follicle (*3*). We sought to dissect the role of Wnt signaling in IFE homeostasis and regeneration. Because tissue stem cells are commonly influenced by signals secreted by nearby "niche" cells (*4*), we examined the presence of Wnts and Wnt inhibitors in the skin.

To determine whether Wnt-responding cells are present in the IFE, we looked in mouse skin for cells expressing *Axin2*, a well-known Wnt/β-catenin target gene. We focused on the mouse hindpaw (plantar) epidermis, a region devoid of hair follicles and sweat ducts (fig. S1A). We marked *Axin2*-expressing cells using Axin2-CreERT2 and found labeled cells in the basal layer (Fig. 1A and fig. S1E), consistent with Axin2 mRNA and reporter gene expression (fig. S1, B to D). These labeled cells generated clones in multiple IFE compartments that persisted for up to a year (Fig. 1A and fig. S1F), demonstrating that Axin2-CreERT2–labeled keratinocytes are self-renewing stem cells.

Recent studies examining epidermal stem cell fate provide little indication of the signaling pathways involved in cell fate choice. Using Axin2-CreERT2 as a combined lineage tracing and Wnt reporter tool, we studied the effect of Wnt signaling on cell fate, by analyzing labeled clones at high resolution in whole-mounted epidermis of Axin2-CreERT2/Rosa26-Rainbow (*5*) mice [Fig. 1B and supplementary theory (ST) section S-II]. We first asked whether long-lived Axin2-CreERT2–labeled clones might derive from slow-cycling stem cells that divide with invariant asymmetry to produce transit-amplifying cells (*6*, *7*), or equivalent "committed progenitors" and stem cells that divide with probabilistic fate (*8*–*10*). If Axin2-CreERT2 labeled only slow-cycling stem cells dividing with invariant asymmetry, we would expect to see labeled single cells that divide rarely and eventually give rise to stable, long-lived clones. In contrast, the probabilistic differentiation and self-renewal of stem cells and committed progenitors would lead to a rapid drop in the number of clones as a result of neutral clonal competition, with a concomitant increase in the average size of persisting clones to compensate for those that are lost (*11*). In addition, within a few cell divisions, the size distribution of the persisting clones would follow a simple exponential curve. Comparing the clonal data to these predictions, we found that the labeled Wnt-responding cells and their progeny exhibited all of the characteristics of probabilistic fate and neutral clonal competition (Fig. 1, C and D; fig. S2, A to C; and ST S-III and S-IV).

To determine whether active Wnt signaling, as indicated by *Axin2* expression, occurs in a functionally distinct subpopulation of IFESCs, we examined the number of Axin2-CreERT2–labeled cells in the basal layer over time. Between 3 days and 5 months after initial labeling, the total number of labeled cells in the basal layer of the epidermis remained constant (Pearson correlation coefficient $R = 0.08$ to time after labeling) (Fig. 1E and fig. S2H). This indicates that both Axin2-CreERT2–labeled and unlabeled cells have equal self-renewal capacity in homeostasis, suggesting that all IFESCs express *Axin2* (fig. S1, B to D), but only a subset is labeled when treated with

[1]Department of Developmental Biology, Howard Hughes Medical Institute (HHMI), Institute for Stem Cell Biology and Regenerative Medicine, School of Medicine, Stanford University, Stanford, CA, USA. [2]Program in Cancer Biology, School of Medicine, Stanford University, Stanford, CA, USA. [3]Department of Bio-engineering, Stanford University, Stanford, CA, USA. [4]Department of Medicine, School of Medicine, Stanford University, Stanford, CA, USA. [5]Department of Systems Biology, Harvard Medical School, Boston, MA, USA.

*Present address: Institute of Medical Biology, A*STAR, Singapore.
†Present address: Swammerdam Institute for Life Sciences, University of Amsterdam, Netherlands.
‡Corresponding author. E-mail: rnusse@stanford.edu (R.N.); allon_klein@hms.harvard.edu (A.M.K.)

Phase Mismatch–Free Nonlinear Propagation in Optical Zero-Index Materials

Haim Suchowski *et al.*

Science **342**, 1223 (2013);
DOI: 10.1126/science.1244303